Study of Debris Throw and Dispersion after Break-up of Reinforced Concrete Structure under Internal Explosion

S. C. Fan[1], Q. J. Yu[1], Y. Yang[1],
H. S. Lim[2], and K. W. Kang[2]

[1] Nanyang Technological University (*E-mail: cfansc@ntu.edu.sg*)
[2] Defence Science &Technology Agency

Presenter : Heng Soon, Lim is a Principal Engineer in DSTA, Singapore. He has been working in the field of explosive safety for the last 10 years and is regular participant in the Klotz Group. Heng Soon holds a Bachelor degree from National University of Singapore and a Masters degree in Civil Engineering from Delft University of Technology.

Abstract

DSTA and NTU have been working together to develop a methodology to simulate the breakup and debris throw of reinforced concrete (RC) structures under internal explosion. The numerical simulation simulates the following phases of responses: internal explosive loading; structural breakup and debris launch; debris primary trajectory and post-impact roll-and-bounce. In last DDESB seminar, our findings on structural breakup process were reported using node-splitting method [1]. In this paper, the focus is on the phases following the structural breakup. As a result of a structural breakup, debris pieces of different sizes are formed and propelled by the blast/gas pressures. When the overpressure subsides, the debris pieces fly under the action of gravity and the air drag. Very often, the debris does not settle at its first landing position. Instead, it impacts the ground and then bounces off and rolls, or even breakup into several smaller pieces. This paper presents the investigation on all these post-breakup processes, including the effects of drag coefficient on the trajectory. Results are plotted in the format of debris dispersion map. Data collected from the Kasun field tests [2] are used for verification. In general, the simulation results are in good accord with the field test results.

1. Introduction

Debris study exists in many fields. Normally, debris study includes these aspects: firstly it is about how debris is produced such as broken part from space shuttle and turbine, wind-borne debris, demolition blast, vehicles transporting explosives, etc. Secondly it is about what the debris flying trajectory is, such as direct prediction of the recycling site of rocket components to maximize the economic benefits, the trajectory of debris from demolition blast to know the estimated safe clearance. And finally, it is about the impact effect of debris on the targets normally known as terminal ballistics, such as the hit results of debris from shell explosion, the hazards of turbine hit by broken debris, space shuttle survival by high speed space debris, wind-borne debris impact on building, et al.

The debris involved in this paper is from the break-up of reinforced concrete structure due to internal explosion. The debris trajectory and dispersion are studied to determine the debris hazard zone which is critical in determining the minimum safe clear distances between magazines and the distances between inhabited buildings and the magazines concerned.

Report Documentation Page

1. REPORT DATE **JUL 2010**	2. REPORT TYPE **N/A**	3. DATES COVERED **-**	
4. TITLE AND SUBTITLE **Study of Debris Throw and Dispersion After Break-up of Reinforced Concrete Structures Under Internal Explosion**		5a. CONTRACT NUMBER	
		5b. GRANT NUMBER	
		5c. PROGRAM ELEMENT NUMBER	
6. AUTHOR(S)		5d. PROJECT NUMBER	
		5e. TASK NUMBER	
		5f. WORK UNIT NUMBER	
7. PERFORMING ORGANIZATION NAME(S) AND ADDRESS(ES) **Nanyang Technological University, Singapore**		8. PERFORMING ORGANIZATION REPORT NUMBER	
9. SPONSORING/MONITORING AGENCY NAME(S) AND ADDRESS(ES)		10. SPONSOR/MONITOR'S ACRONYM(S)	
		11. SPONSOR/MONITOR'S REPORT NUMBER(S)	
12. DISTRIBUTION/AVAILABILITY STATEMENT **Approved for public release, distribution unlimited**			
13. SUPPLEMENTARY NOTES **See also ADM002313. Department of Defense Explosives Safety Board Seminar (34th) held in Portland, Oregon on 13-15 July 2010, The original document contains color images.**			
14. ABSTRACT			
15. SUBJECT TERMS			

16. SECURITY CLASSIFICATION OF:			17. LIMITATION OF ABSTRACT **SAR**	18. NUMBER OF PAGES **33**	19a. NAME OF RESPONSIBLE PERSON
a. REPORT **unclassified**	b. ABSTRACT **unclassified**	c. THIS PAGE **unclassified**			

In last DDESB seminar, our findings on structural breakup process were reported using node-splitting method. Similar methodology for the simulation of masonry wall failure and debris scatter due to high explosive loading by LS-DYNA was developed [3]. In this paper, the focus is on the phases following the structural breakup. As a result of a structural breakup, debris pieces of different sizes are formed and propelled by the blast/gas pressures. When the overpressure subsides, the debris pieces fly under the action of gravity and the air drag. Very often, the debris does not settle at its first landing position. Instead, it impacts the ground and then bounces off and rolls, or even breakup into several smaller pieces. This paper presents the investigation on all these post-breakup processes, including the effects of drag coefficient on the trajectory. Results are plotted in the format of debris dispersion map. Data collected from the Kasun field tests are used for verification.

2. Debris formation

In Quantity-Distance (QD) model [4], the characteristics of the debris, like the initial velocity and mass of the debris, are obtained from input probability distribution, such as, the debris mass distribution is assigned to be exponential. The debris initial velocity and angle distributions are assigned to be normal. While in present study, the debris information such as mass, size, ejection position, velocity and angle are retrieved according to certain algorithms (Seen in Appendix A) based on break-up simulation output by LS-DYNA.

3. Debris flying trajectory

3.1 Drag force

The general equation for the drag force is[5]:

$$F_d = \frac{1}{2} C_d \rho_a A V^2 \tag{3.1}$$

where C_d is drag coefficient, ρ_a is air density, V is velocity of the flying object, A is the object's cross-sectional area. In this study, A is defined as debris' maximum sectional area perpendicularity to the motion direction. The equation means that the drag force is proportional to the drag coefficient, the air density, the normal sectional area, and the square of the velocity.

In the following, a new parameter k is introduced, and Eq. 3.1 is re-written as[6],

$$F_d = mgkv^2, k = \frac{\rho_a A}{2mg} C_d \tag{3.2}$$

3.2 Equations of debris motion

When spinning motion is excluded, the translational motion of debris can be described by the motion of its centre. The forces acting on the debris are the gravitational force and drag force only. The gravitational force acted on a debris mass m is constant, while the drag force F_d is varying and is proportional to the square of the velocity. The kinematic relationship between acceleration a, velocity V and position (x,y) can be expressed in differential equations. Hence, the debris motion is governed by the differential equations as follow[6]:

$$a = \frac{dV}{dt} = -g \sin\theta - gkV^2 \quad , \quad \varphi = \frac{d\theta}{dt} = -g \frac{\cos\theta}{V} \tag{3.3}$$

$$V_x = \frac{dx}{dt} = V \cos\theta \quad V_y = \frac{dy}{dt} = V \sin\theta$$

Here, V is the velocity of the debris, θ is the slope of the trajectory to the horizontal, g is the acceleration due to gravity, x and y are the Cartesian coordinates of the debris. The basic parameters involved in the debris trajectory calculation are shown in Fig. 1:
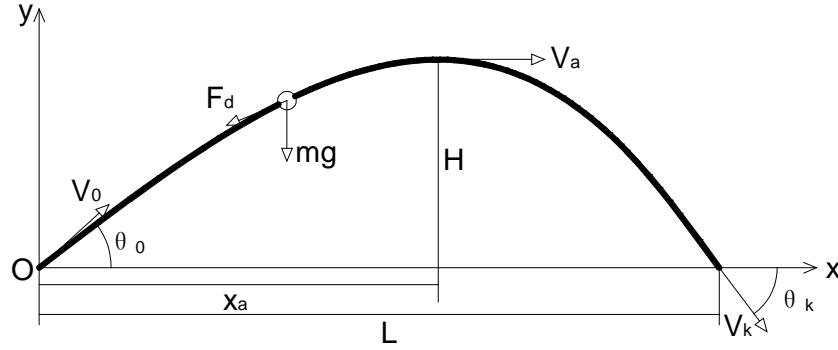

Fig. 1   Basic parameters of trajectory [6]

Here, V_0 and θ_0 are the initial or the projective velocity and angle of the debris; V_k and θ_k are the landing velocity and angle when debris hits the ground; V_a and x_a are the velocity and horizontal displacement when debris gets to the vertex of the trajectory; H is the vertex height; L is the debris horizontal displacement before it hits the ground.

To solve Eqs (3.3), we divide the trajectory path into a series of small intervals $[\theta_0, \theta]$, then the whole trajectory could be traced step by step based on the equations 3.4 [6].

$$V(\theta) = \frac{V_0 \cos\theta_0}{\cos\theta \sqrt{1 + kV_0^2 \cos^2\theta_0 (f(\theta_0) - f(\theta))}} \quad , \quad f(\theta) = \frac{\sin\theta}{\cos^2\theta} + \ln tg\left(\frac{\theta}{2} + \frac{\pi}{4}\right) \tag{3.4}$$

$$x = x_0 + \frac{V_0^2 \sin 2\theta_0 - V \sin\theta}{2g(1+\varepsilon)} \quad , \quad y = y_0 + \frac{V_0^2 \sin^2\theta_0 - V^2 \sin^2\theta}{g(2+\varepsilon)} \quad , \quad \varepsilon = k(V_0^2 \sin\theta_0 + V^2 \sin\theta)$$

These simple analytical formulae of Equations 3.4 enable recurrent computation of the main parameters of motion: H, V_a , x_a , L, x_a, V_k , θ_k , the time of ascent t_a and the total motion time t[6].

3.3 Determination of drag coefficient C_d

The drag coefficient C_d is a number that aerodynamicists use to model all of the complex dependencies of shape, surface roughness, and flow conditions on moving object drag. This dimensionless value quantifies the drag or resistance of an object in a fluidic environment such as air or water. The higher the C_d, the higher aerodynamic or hydrodynamic drag force the moving body will experience [7].

The value of drag coefficient C_d is a function of the shape of object and also the Reynolds number (*Re*). The dimensionless number *Re* is defined by $\text{Re} = \rho l v / \eta$ where

l represents the characteristic length scale of the object in the cross-sectional plane and η the dynamic viscosity of the medium. In the present study, to describe the debris free flying motion, it is necessary to assess its range of Re. The air density ρ is assumed to be constant, $\rho=1.293$ kg/m^3. So is the viscosity of air (use the value $\eta=1.78\times10^{-5}$ kg/(m·s) at 15°C). As such, the Reynolds number will be proportional to the characteristic size of debris (l) and the velocity (v). To estimate the lower bound of Re, set $l_1 = 0.01$m and $v_1 = 10$ m/s; while for the upper bound, set $l_2 = 0.20$ m and $v_2 = 500$ m/s. Thus the Re lies in the range of $[7.3\times10^3 \sim 7.3\times10^6]$.

Fig. 2a shows the typical relationship between the drag coefficient C_d and the Reynolds number Re for a sphere with smooth surface [8]. As can seen from the figure, C_d is less than 1 when Re is greater than 10^2; and C_d is about 0.5 when Re lies in the interval $[10^3$, $3\times10^5]$. The sudden drop of C_d, when Re is about 4×10^5, is due to the drag crisis (which is associated with the change of the boundary layer on the sphere's surface from laminar to turbulent). From [9] it is observed that the rough surface causes the drag crisis shift to a smaller Re interval, accompanying the increase of the minimum C_d.

Fig. 2b shows curves of the drag coefficient versus Re number for circular cylinder and square cylinder [9]. It can be seem that the square cylinder has overall drag coefficient higher than the circular one. Further, the square cylinder totally skips the drag crisis.
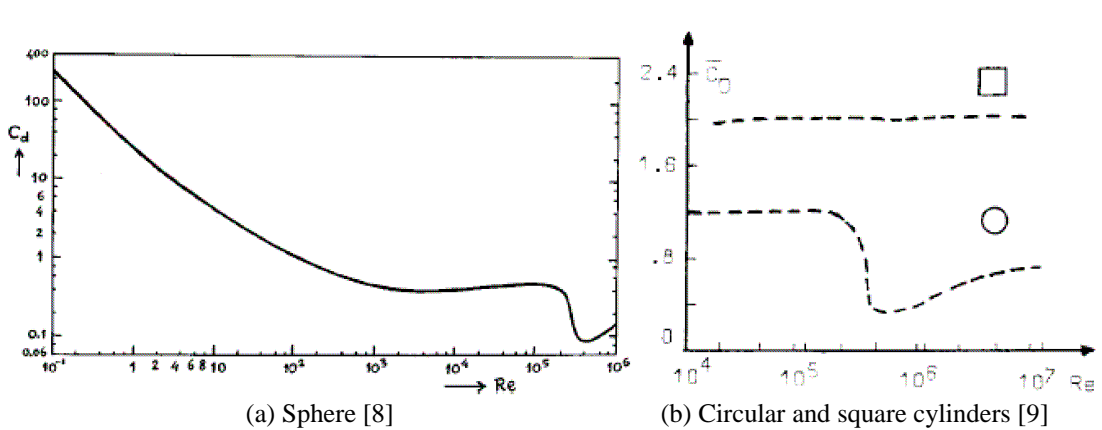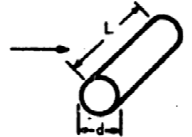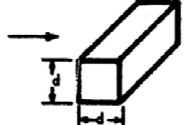

| (a) Sphere [8] | (b) Circular and square cylinders [9] |

Fig. 2   Drag coefficient versus Reynolds number

In the present debris study, the formed concrete debris will be in multi-angular irregular shape with serious roughness. To adopt a reasonable C_d value for present study, values for three benchmark shapes or surfaces are further considered as shown in Table 1.

Table 1 Drag coefficient C_d [10]

OBJECT	C_d		REYNOLDS NO. RANGE	CHARACTERISTIC LENGTH	CHARACTERISTIC AREA
SPHERE	$24 (N_R)^{1/2}$		$N_R < 1$		
	0.47		$10^3 < N_R < 3 \times 10^5$	d	PROJECTED AREA
	0.2		$N_R > 3 \times 10^5$		
CIRCULAR CYLINDER	L/d		$10^3 < N_R < 10^5$		
	1	0.63			PROJECTED
	5	0.8		d	AREA
	10	0.83			
	20	0.93			
	30	1.0			
	∞	1.2			
SQUARE CYLINDER	2.0		$3.5 (10)^4$	d	PROJECTED AREA

The values for the spherical shape are in generally the smallest, while the values for the circular and square cylinders are higher. As the debris shape will never be a perfect smooth circular cylinder but multi-angular, it makes sense to assume that the drag coefficient for debris is closer to that for the square cylinder, whose value is independent of aspect ratio (L/D). Again, the multi-angular shape of debris is somehow between the circular and the square. Based on the weakening trend of drag crisis for rough surface and totally skip of the drag crisis for square cylinder, it is reasonable to assume that the drag coefficient for the debris remains more or less constant against the Reynolds number in the our interested range $[7.3 \times 10^3 \sim 7.3 \times 10^6]$. Consider the value C_d =0.7 for a circular cylinder having aspect ratio (L/D) of 2, and the value C_d =2.0 for a square cylinder of any aspect ratio. It is supposed that the formed debris has the transitional shapes from the smooth circular (C_d =0.7) to the blunt square (C_d =2.0). In the absence of experimental data, values of drag coefficient for the intermediate shapes are assumed. The octagonal shape is assumed 1.2; while the hexagonal is 1.6 as shown in [10]. So the range ($1.2 < C_d < 2.0$) seems fit for the current interest.

3.4 Effects of C_d on debris trajectory

Fig. 3 shows different debris trajectories when using varied drag coefficient C_d (0~2.0). The debris is assumed to be 0.2 kg having launch velocity of 100m/s at an angle 5° with the horizon. It can be seen that value of C_d has significantly effect on the debris trajectory. Lower C_d leads to larger travel distance and it is more prominent when C_d is less than 1.0. For the range ($1.2 < C_d < 2.0$) of current interest, the travel distance when using lower one (C_d =1.2) is about 101m; while using the higher one (C_d =2.0) is about 81m, which is approximately 81% of 101m. Empirically, C_d =1.2 is chosen in the current study. It is worth noting that in QD model the input for the drag coefficient is a uniform distribution varying between 1.0 and 2.0[4].
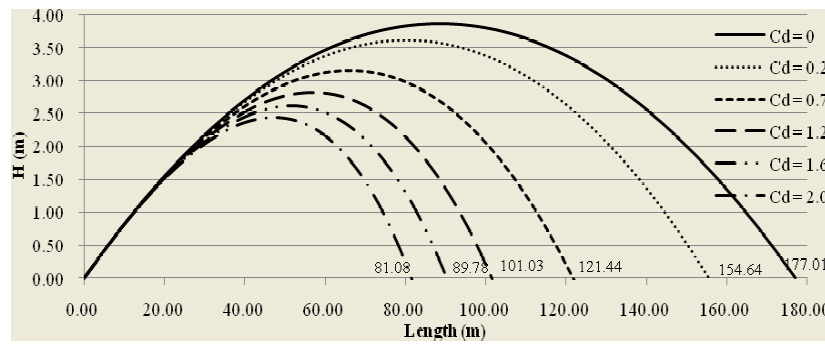
Fig. 3 Debris Trajectories by various C_d (m = 0.2 kg, V_0 = 100 m/s, θ_0 = 5°)

3.4 Size effect on C_d

The presence of drag force leads to size effect on the trajectory because mass is proportional to volume of debris while drag force is proportional to the square of the square of the cross-sectional area. With the same initial launching conditions ($v_0 = 60 m/s$, $\theta_0 = 20°$) and using the same drag coefficient $C_d = 1.2$, Fig. 4a shows the debris travelling distance against debris mass. The relationship appears to be hyperbolic. For smaller debris, the travelling distance increases almost linearly with the debris mass, but for larger debris, the rate of increases is seen reduced drastically due to stronger drag. Note that if drag is absent (C_d =0), the travelling distance should be the same for all debris.
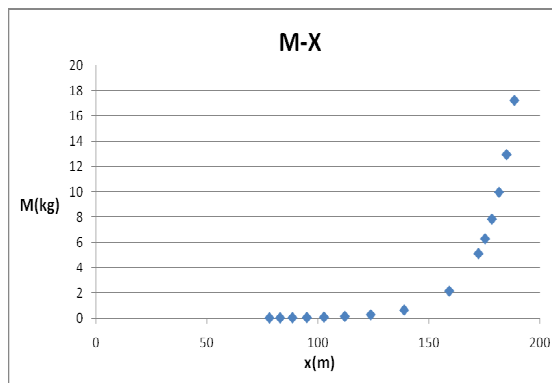
(a) Travelling distance vs. debris' mass
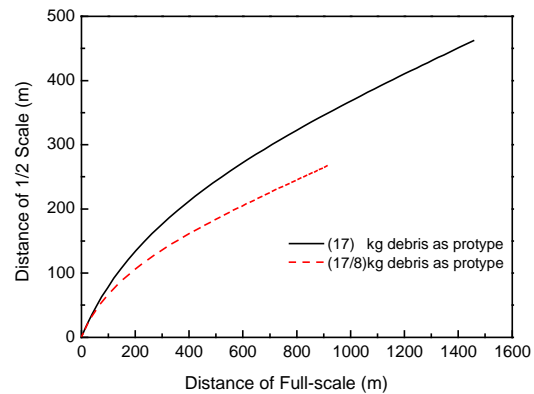
(b) Distance relation between scaled debris

Fig. 4 Size effect on C_d

To illustrate the size effect, two pieces of prototype debris are used. The first is a 17-kg debris and the second one is a (17/8)-kg debris. The travelling distances for each prototype debris and its half-scale debris for a series of launch velocities are computed. Their relationship are plotted in Fig. 4b. Two distinct curves are seen. It illustrates the size effect that the relationship depends on the mass of the protype debris.

3.6 Debris bounce

If debris hit the ground at a shallow angle, it will bounce. In this study, debris bounce is considered according to the criterion [11] below.
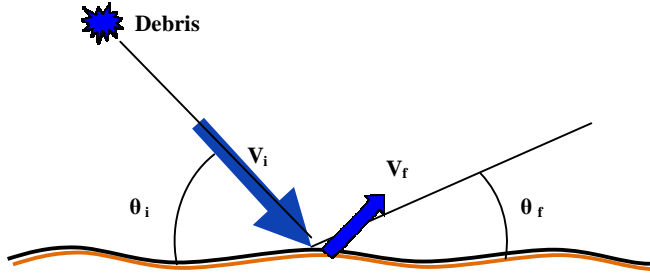

Fig. 5   Parameters in debris bounce

$$V_f = 0 \; ; \; \theta_f = 0 \qquad\qquad\qquad \text{for } \theta_i \geq 13° \text{ and } V_i \geq 18 m/s \qquad (3.5)$$

$$V_f = (1.0 - 0.00476\theta_i)V_i \; ; \; \theta_f = 0.484\theta_i \qquad \text{otherwise}$$

V_i is the velocity of the debris before impact, θ_i is the impact angle, measured from the ground up, V_f is the post-impact rebound velocity and θ_f is the post-impact rebound angle also measured from the ground up.

In this study, the total travelling distance of debris is limited to a maximum of two bounces (if applicable) since the effect of the further bounces becomes insignificant.

3.7 Dispersion map

Debris dispersion map can provide the detailed distribution of debris settled down on ground. It reveals the debris distribution in radial and circumferential directions. The dispersion maps are presented in two forms. The first is plotted against the absolute debris number. The second is plotted against the normalized number (which is defined as debris number per m^2 in a cell, namely debris density). The debris density is often used as a parameter to evaluate the debris hazard. The dispersion map can be used to assess the hazard zone and Inhabited Building Distance (IBD).

3.8 Hazard zone and IBD

The ultimate objective of this study on debris is to address the operational need with regard to the safety/hazard zone around a magazine. It is to establish some guidelines for identifying safe zone against the hazardous debris. A piece of debris having kinetic energy (= ½ mv^2) of more than 79 J is considered hazardous or lethal. The hazard zone is defined as a patch of area on plan such that the lethal threat level exceeds one hazardous piece of debris per 56 m^2[12]. A hazard zone can be of any shape as long as it envelopes all hazardous patches. The IBD is an index radius of the smallest circle that encompasses the hazard zone totally as shown in Fig. 6.
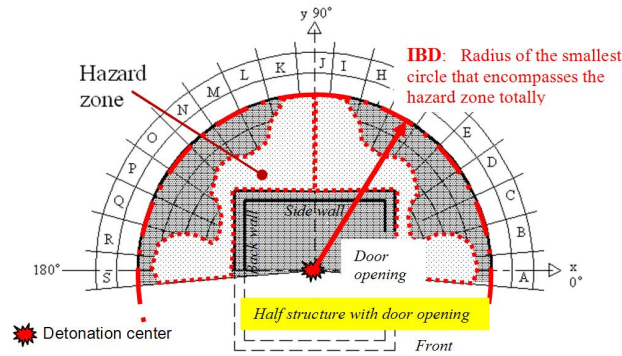
Fig. 6   Hazard zone and IBD

4. Case study

This section presents the illustrative modeling of debris throw after an RC magazine break-up subjected to internal blast load. Fig. 7a is the filed test physical object in Kasun II tests No. 2[2]. Fig. 7b is the simulation model for half of the test object. Internal dimensions of the cubic box-shape RC structure are 2.0m x 2.0m x 2.0m. Wall and roof are of 0.15m thick and are reinforced with Ø 12 mm bars at 100 mm centers in two directions having double layers. The charge weight is 20 kg-equivalent TNT having a loading density of 2.5 kg/m^3.

4.1 Simulation model

| (a) The field test object [2] | (b) Simulation model |
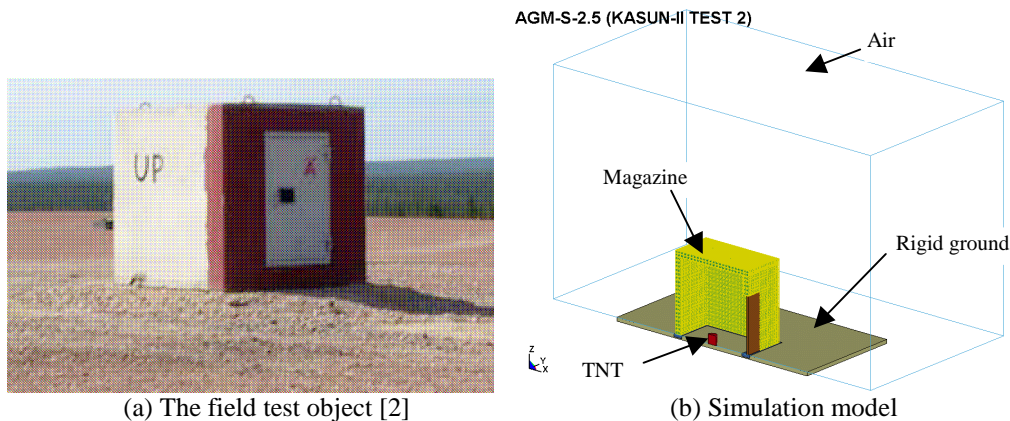
Fig.7   Field test object and numerical model

This physical domain is modeled by finite elements. The finite element model includes discretization of the solid magazine structure and the air space inside and outside. Due to symmetry, only half-structure model is built to save calculation cost and the symmetry plane locates at the X-Z plane as can be seen in Fig. 7b.

4.2 Comparison of simulation results with field record from Kasun Test

4.2.1 Comparison of launch velocity and angle distribution

Launch velocity is an important parameter in debris hazard study. Figs. 8a and b show the launch velocity and angle distribution respectively obtained from simulation. Corresponding results obtained from field test are plotted in Figs. 8c and 8d. Launch angle is measured from the horizontal plane. Upward is positive; downward is negative. The launch angle varies within the range [-5°, 90°] and sorted at 5° intervals. Note that

if drag force is absent, the maximum horizontal travelling distance is derived from debris having launch angle of 45 degree. With the presence of drag force, the maximum distance should be derived from debris having launch angle lower than 45 degree.
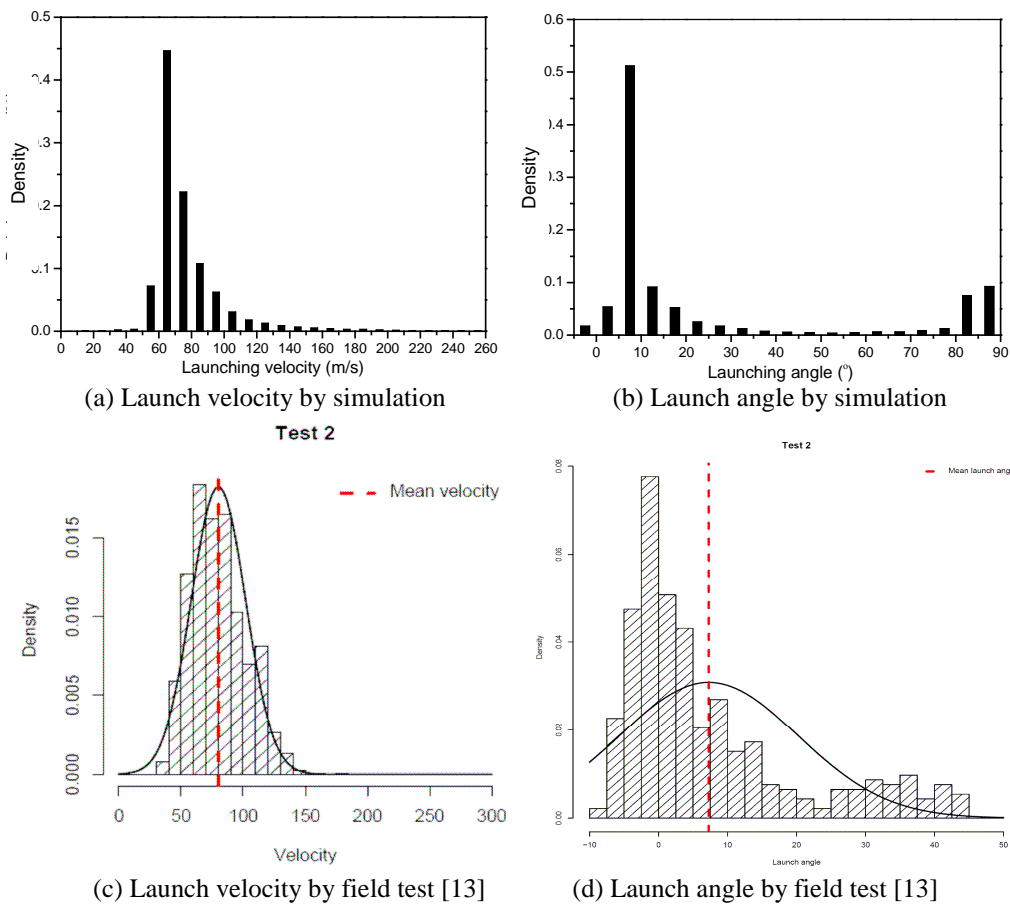

(a) Launch velocity by simulation

(b) Launch angle by simulation

(c) Launch velocity by field test [13]

(d) Launch angle by field test [13]

Fig. 8   Comparison of launch velocities and angles

It can be seen from Fig. 8a that majority of debris has launch velocity in the range of [50, 100] m/s, and has the highest density (about 45%) lies in the range of [60, 70] m/s; also from Fig. 8b that launch angles have two clouds (71% and 17%) in the ranges [0°, 20°] and [80°, 90°], respectively, with the highest density (51%) occurred in the range of [5°, 10°]. Further scrutinizing reveals that debris having low launch angle are mostly derived from the walls and debris having high launch angle are mostly derived from the roof. Note that Figs. 8c and 8d are the probability density function of launch velocity and angle deduced from high speed video record of the field test, but limited to visible debris having launch angle not more than 45°. It can be seen from Fig. 8c that the velocities are nearly of normal distribution with a mean velocity of about 80m/s, which is comparable with the actual [13] mean velocity of 61m/s. Comparisons of launch velocity distributions in Fig.8 show that simulation results agree well with field test record. However, the launch angle distributions only poorly agree though the trends seemingly match. Nevertheless, when field data are poorly fit to a normal distribution, it yields a mean angle of 7°, which agrees well with the simulation results and also the Klotz group recommendation [13] of 5° with a standard deviation of ±6° (as adopted in the prediction tool, namely 'KG-ET'), having 95% of debris in the range of [-7°, +17°].

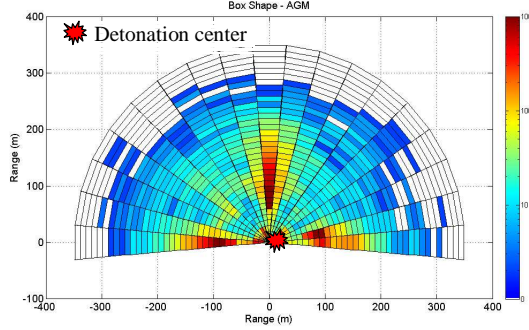4.2.2 Comparison of dispersion and hazard zone

Numbers of debris pieces finally settled on ground are counted in 19 equal sectors, namely Sector A to Sector S over a 190-degree plan view as shown in Fig. 9a. The angle of each sector is 10 degrees, with the first one starting from -5° and the last one ending at 185°. Along the radial direction, each sector has 10m interval. Fig. 9a depicts the collection sectors. In the real field test, it is a very tedious and hard work to collect all the debris. To alleviate the hardship, the debris collation is not exhaustive and only those debris pieces having mass greater than 0.055kg were collected during the Kasun field test. Fig. 9b plots the dispersion map from the Kasun test data. Fig. 9c shows the debris dispersion map obtained from simulation which includes the effect of bouncing twice after first impact. It should be noted that the smallest minute-sized debris pieces obtained in simulation are all about 0.065 kg. Moreover, the counting of debris in the simulation is exhaustive. Against this background, it will not be surprised to see the non-matching comparison between the simulation and field test data. Nevertheless, the same trend of having high density in Sectors A, J and S (in the direction normal to the walls) are observed. Also, the maximum debris throw distance agrees well.
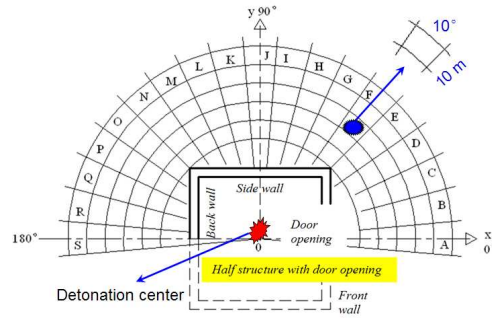
(a) Diagram of debris collection sectors
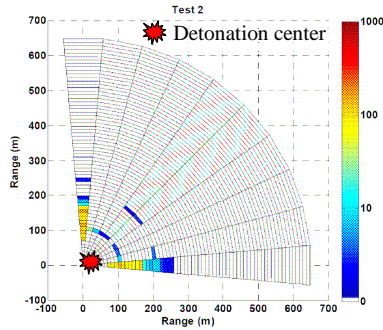
(b) Map from Kasun data[2]   (c) Map obtained from simulation including twice bounce

Fig. 9 Comparison of debris dispersion map

From the dispersion map, the hazard zone can be deduced. The map of hazard zone is shown in Fig. 10. The hazard zone with high hit probability is normal to the walls, and this is consistent with the dispersion map. Table 2 gives the comparison of IBD. The IBD value along sector J is close to the field test result, but not that along sector S where the IBD value is less than that of test result. It is worth noting that the field test results are derived from the assumption which regards all collected debris as hazardous and lethal due to lacking of velocity data. This would lead to higher estimation of IBD.
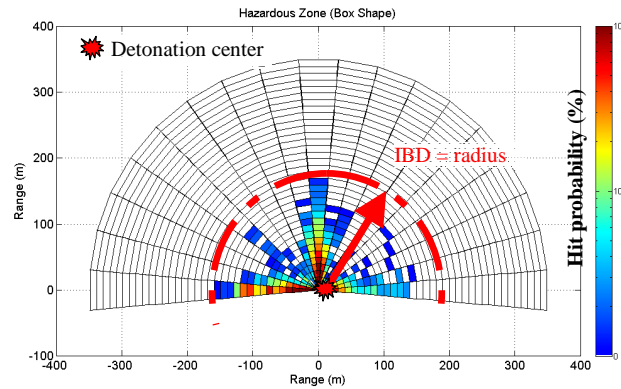
Fig. 10   Map of hazard zone

Table 2 Comparison of IBD (m)

	Sector A (Front wall)	Sector J (Side wall)	Sector S (Back wall)	Global (Max)
Simulation	140	170	160	170
Kasun test[2]	-	180	220	220

5. Conclusion

In this paper, study of debris throw and dispersion after break-up of reinforced concrete structure under internal explosion is presented. The debris formation algorithm, debris motion trajectory including the effect of air drag, and debris bounce are investigated. The debris launch velocity and launch angle distribution, debris dispersion map and IBD determination are analyzed and compared with Kasun field test results. In general, the simulation results are in good accord with the field test results.

Reference

1. Yu, Q. J., Yang, Y. W., Fan, S.C., Lim, H. S. and Koh, Y. H.. A Novel Numerical Approach for Modeling Break-up of Reinforced Concrete Structure, 33rd DoD Explosive Safety Seminar, Palm Springs, California, 2008.
2. Berglund R., Carlberg A., Forsen R. etc. Langberg. Break up tests with small "ammunition houses". FOI-R--2202—SE, Forsvarsbygg Report 51/06, Technical report, Dec 2006.
3. McCallum, S. C., Locking, P. M. and Harkness, S. R.. Simulation of masonry wall failure and debris scatter. 6th European LS-DYNA User's Conference, 2008.
4. Department of Defense Explosives Safety Board (DDESB), Prediction of Building Debris for Quantity-Distance Siting [R].T.P.13 1991.
5. Landau L. D. and Lifshitz, E. M.. Fluid Mechanics. Oxford, U.P., New York, 1959.
6. Chudinov P. S.. The motion of a point mass in a medium with a square law of drag. J. Applied Mathematics and Mechanics, 2001, 65(3): 421-426.
7. Clancy, L. J.. Aerodynamics. London Pitman, 1975.
8. Timmerman P. and Jacobus P. van der Weele. On the Rise And Fall of a Ball with Linear or Quadratic Drag. Am. J. Phys. 1999, 67(6): 538-546.
9. Barr, C. and Barnaud, G.. High Reynolds number simulation techniques and their application to shaped structures model test. Journal of Wind Engineering and Industrial Aerodynamics, 1995, 57(2-3): 145-157.
10. Lee, A. J. H. . A general study of tornado-generated missiles. Nuclear Engineering and Design, 1974, 30: 418-433.
11. Knock C., Horsfall I., Champion S.M. et al. The bounce and roll of masonry debris. International Journal of Impact Engineering, 2004, 30: 1-16.

12. AASTP-1 (Allied Ammunition Storage and Transport Publication 1). Manual of NATO safety principles for the storage of military ammunition and explosives, May 1992.
13. Geir Arne Gronsten, Rickard Forsen, Roger Berglund. Kasun-II debris velocity-summary of findings. Forsvarsbygg and FOI material. 2008.

Appendix A: Debris formation algorithm

A.1 Element displacement and velocity after break-up

The information on displacement and velocity of all nodes during break-up process is stored in the output file named *NODOUT* in sequence of intervals Δt_s. Thus for a given time t, the displacement u^{ECt} and velocity v^{ECt} of an element center is the average value of its 8 corner nodes, which are represented as

$$u^{\mathrm{EC}t} = \frac{1}{8}\sum_{i=1}^{8} u_i^t \tag{A.1}$$

$$v^{\mathrm{EC}t} = \frac{1}{8}\sum_{i=1}^{8} v_i^t \tag{A.2}$$

where u_i and v_i are the displacement and velocity of the ith node in this element at time t.

A.2 Debris definition from the recovered eroded- element pool

From the information recorded in the file named *MSSG* for the eroded elements, the element number and its erosion time can be retrieved. The index set of erosion elements are represented by Φ^{EE}. All the eroded elements in the record will be grouped according to the sequence of time intervals. G_j^{EE} and t_j^{GE} are, respectively, the jth eroded element group and its erosion time.

$$\phi^{\mathrm{EE}} = \left\{ i \middle| \mathrm{Ele}\ i \ \text{has eroded},\ i = 1,\ 2,\ \cdots,\ N^{\mathrm{TE}} \right\} \tag{A.3}$$

$$G_j^{\mathrm{EE}} = \left\{ i \middle| t_i^{\mathrm{EE}} - t_j^{\mathrm{GE}} \le \Delta t^{\mathrm{GE}}, i \in \phi^{\mathrm{EE}} \ \text{and}\ i = 1,\ 2,\ \cdots,\ N^{\mathrm{TE}} \right\} \tag{A.4}$$

$$\begin{cases} t_1^{\mathrm{GE}} = \min\left(t_i^{\mathrm{EE}}\right) \middle| i \in \phi^{\mathrm{EE}} \ \text{and}\ i = 1,\ 2,\ \cdots,\ N^{\mathrm{TE}} \\ t_j^{\mathrm{GE}} = \min\left(t_i^{\mathrm{EE}}\right) \middle| t_i^{\mathrm{EE}} > t_{j-1}^{\mathrm{GE}} + \Delta t^{\mathrm{GE}}, i \in \phi^{\mathrm{EE}} \ \text{and}\ i = 1,\ 2,\ \cdots,\ N^{\mathrm{TE}} \end{cases} \tag{A.5}$$

where t_i^{EE} is the erosion time of element i, Δt^{GE} is a specified interval.

For each eroded element group, we can obtain the number and size of debris through checking initial inter-element connection. Consequently, debris can be defined from the eroded-element pool. It should be noted that the recorded erosion time of one element actually may not be the same as its physical break-up time.

A.3 Debris definition from the un-eroded-element pool

For un-eroded elements, the current distance of any nodal pair, which is at the same location but tied over the interface between two neighboring elements in the initial state, can be obtained from the results of last time step. If the distance is greater than a

specified maximum distance d_{max}^{cpp}, the pair of nodes splits (i.e., the constrained nodes tie between the two nodes is released). Note that two neighboring elements may still tie together if only one of their nodal pair splits (or separates) since there are 4 nodal pairs between them in 3D (i.e., the whole interface between the two elements does not fracture). If fracture does occur, the two neighboring elements separate. Thereby for a given element, we can loop through its surfaces to obtain an initial fragment. Upon repeatedly looping and checking the current disconnection of all tied nodal pairs along the outer surface of a sub-region, the possible formation of a piece of debris can be identified, and eventually a final form of fragment (or debris) is obtained when no other elements are tied to it. By treating the un-eroded elements in this way, we can define the sizes of fragments (or debris), formed from the mass of un-eroded elements.

A.4 Debris ejection position and ejection velocity

Once the sizes of debris are defined, other physical and kinetic properties of debris can be derived from the information of its component elements. An individual debris' initial center $P^{FC}(x, y, z)$, mass M^F, volume V^F, displacement u^{FCt} and velocity can be defined as follow.

$$P^{FC}\left(x,y,z\right) = \frac{1}{n^{FE}}\sum_{i=1}^{n^{FE}}P_i^{EC}\left(x,y,z\right)$$

(A.6)

$$V^F = \sum_{i=1}^{n^{FE}}V_i^E$$

(A.7)

$$M^F = \sum_{i=1}^{n^{FE}}\rho_i^E V_i^E$$

(A.8)

in which, $P_i^{EC}(x, y, z)$, V_i^E, and ρ_i^E, respectively, represents the initial center, volume and medium density of the ith element in the fragment including n^{FE} elements. For 3D solid brick elements used in this computation, the initial center of any element is given as

$$P^{EC}\left(x,y,z\right) = \frac{1}{8}\sum_{i=1}^{8}P_i\left(x,y,z\right)$$

(A.9)

where $P_i(x, y, z)$ is the coordinates of the ith node in the element.

Considering a single debris, it is reasonable to evaluate its value at the centre by taking the arithmetical mean of values from all its component elements. The values of central displacement u^{FCt} and velocity v^{FCt} are defined as follow.

$$u^{FCt} = \frac{1}{n^{FE}}\sum_{i=1}^{n^{FE}}u_i^{ECt}$$

(A.10)

$$v^{\mathrm{FC}t} = \frac{1}{n^{\mathrm{FE}}} \sum_{i=1}^{n^{\mathrm{FE}}} v_i^{\mathrm{EC}t}$$

$$(A.11)$$

By summing up the initial position and the displacements u^{FCt} in all time steps, from the initial till the last time step, one can get the final position of an individual fragment, and it is its ejection position. Similarly, one can get the ejection velocity for an individual fragment. These two values are taken as the initial condition in debris free-flying motion.

Study of Debris Throw and Dispersion after Break-up of Reinforced Concrete Structure under Internal Explosion

Presentation by Heng Soon, Lim

S.C. Fan[1], Q.J.Yu[1], Y.W. Yang[1], H.S. Lim[2] and K.W. Kang[2]
1 Nanyang Technological University (NTU), Singapore
2 Defence Science and Technology Agency (DSTA), Singapore

20-Jul-10

Outline

- ❖ Background
- ❖ Debris trajectory
- ❖ Parametric study on drag coefficient
- ❖ Case study
- ❖ Future works

Background

Internal Blast Loading → Response & Breakup of Structure → Debris Launch → Debris Trajectory → Post Ground Impact

Debris trajectory

Post impact trajectory

Debris Distribution Map

Debris distribution map
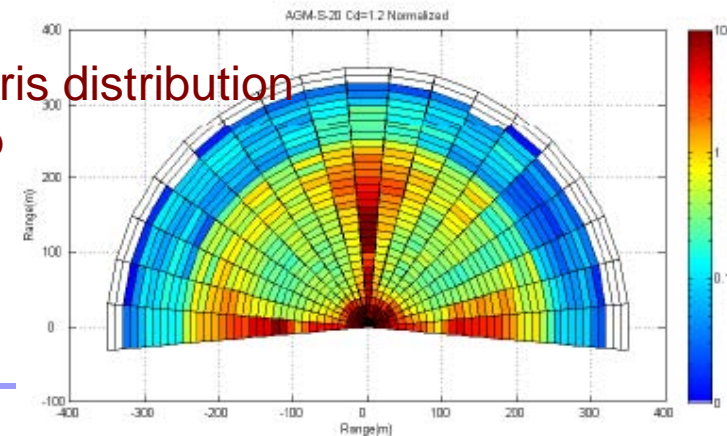
Debris Trajectory

Assumptions

• Each debris flies independently as a singular body.

• Ignore spinning motion of debris.

• Only drag forces and gravitational forces acting on the debris.
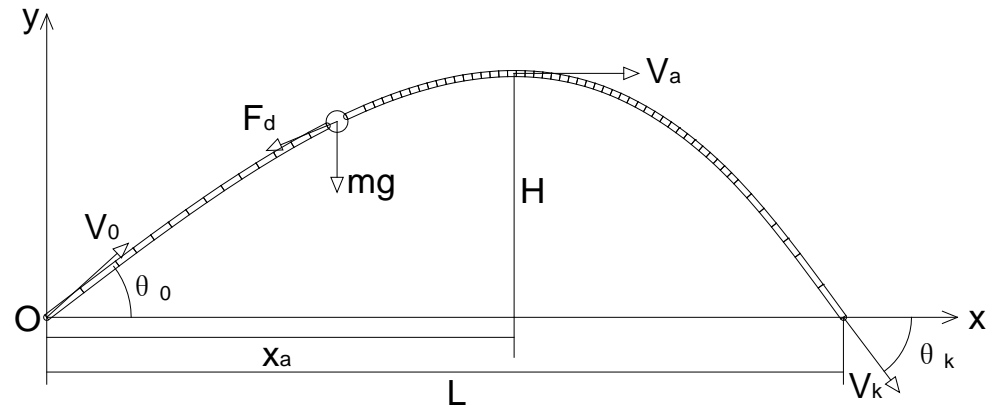
Drag force

$$F_d = \frac{1}{2} C_d \rho_a A V^2$$

or

$$F_d = mgkv^2 \qquad k = \frac{\rho_a A}{2mg} C_d$$

Equations of Motion

$$x = x_0 + \frac{V_0^2 \sin 2\theta_0 - V \sin \theta}{2g(1+\varepsilon)}$$

$$y = y_0 + \frac{V_0^2 \sin^2 \theta_0 - V^2 \sin^2 \theta}{g(2+\varepsilon)}$$

$$a = \frac{dV}{dt} = -g \sin \theta - gkV^2$$

$$\varphi = \frac{d\theta}{dt} = -g \frac{\cos \theta}{V}$$

$$V_x = \frac{dx}{dt} = V \cos \theta$$
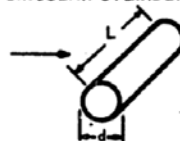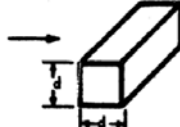
$$V_y = \frac{dy}{dt} = V \sin \theta$$

$$\varepsilon = k(V_0^2 \sin \theta_0 + V^2 \sin \theta)$$

Determination of drag coefficient C_d

- Based on existing literature.

- Mostly smooth surface with regular shapes.

- Reynolds Number, range of interest : $7.3 \times 10^3 - 7.3 \times 10^6$

- Smooth cylinder $C_d = 0.7$ (aspect ratio of 2)

- Square cylinder $C_d = 2.0$ (any aspect ratio)

- Debris with irregular shapes in between the 2 values.

➔ Assume $1.2 < C_d < 2.0$

OBJECT		C_d		REYNOLDS NO. RANGE	CHARACTERISTIC LENGTH	CHARACTERISTIC AREA
SPHERE		$24 (N_R)^{\frac{1}{2}}$		$N_R < 1$		
		0.47		$10^3 < N_R < 3 \times 10^5$	d	PROJECTED AREA
		0.2		$N_R > 3 \times 10^5$		
CIRCULAR CYLINDER	L/d			$10^3 < N_R < 10^5$		
	1	0.63				PROJECTED AREA
	5	0.8			d	
	10	0.83				
	20	0.93				
	30	1.0				
	∞	1.2				
SQUARE CYLINDER		2.0		$3.5 (10)^4$	d	PROJECTED AREA

Reynolds Numbers & drag coefficient
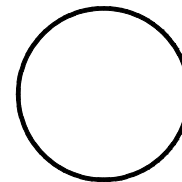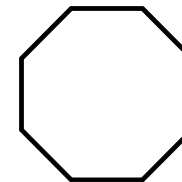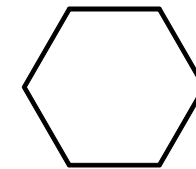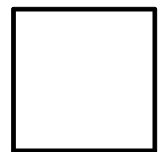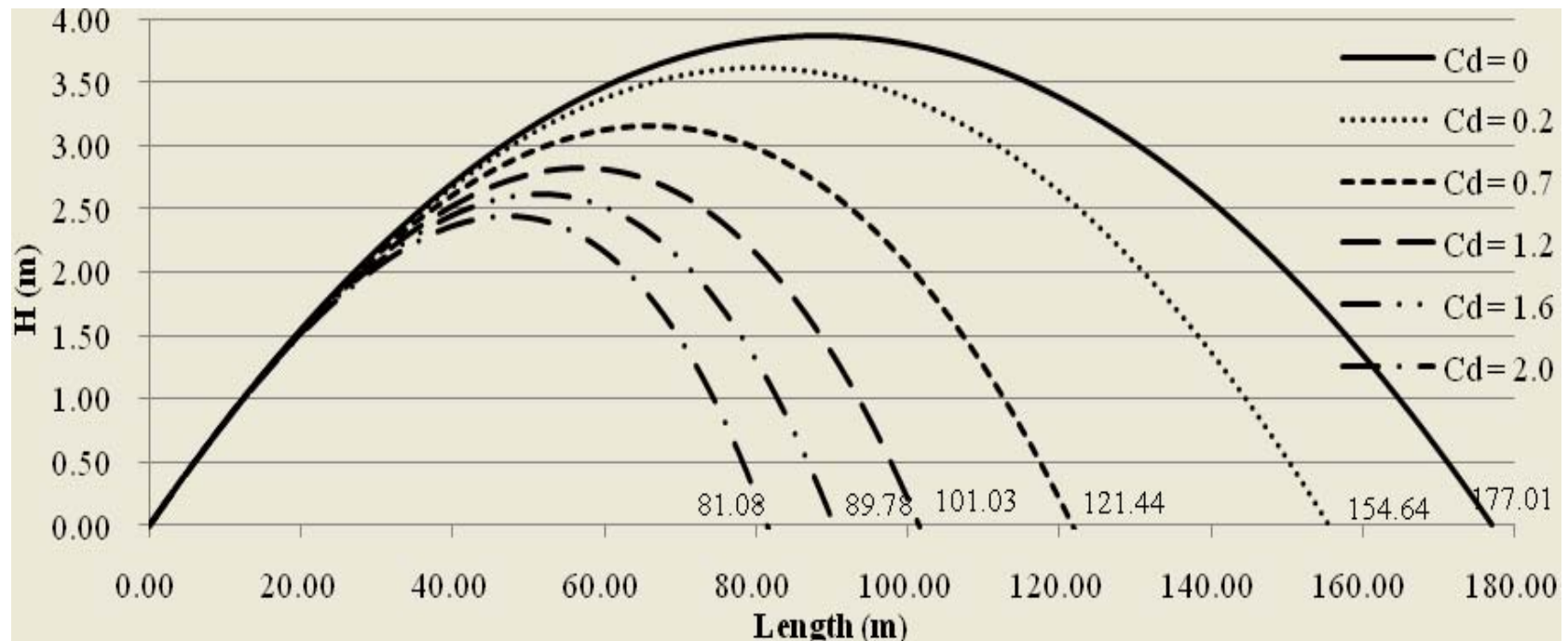

Cd = 0.7   Cd = 1.2   Cd = 1.6   Cd = 2.0

Effects of C_d on debris trajectory
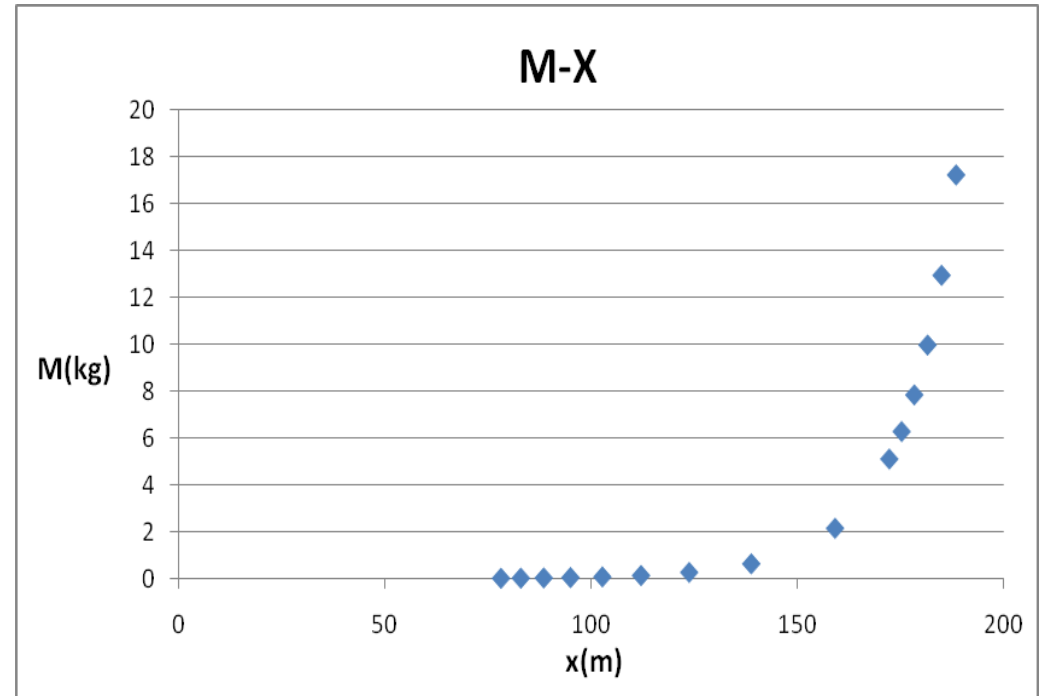

Debris Trajectories by various C_d (m = 0.2 kg, V_0 = 100 m/s, θ_0 = 5°)

→ Final debris range is very sensitive to drag coefficient !

Size Effect on C_d

- Study the sensitivity of debris size & mass on debris range.

- Initial launch conditions : $v_0 = 60$m/s, $\theta_0 = 20^0$, $C_d = 1.2$

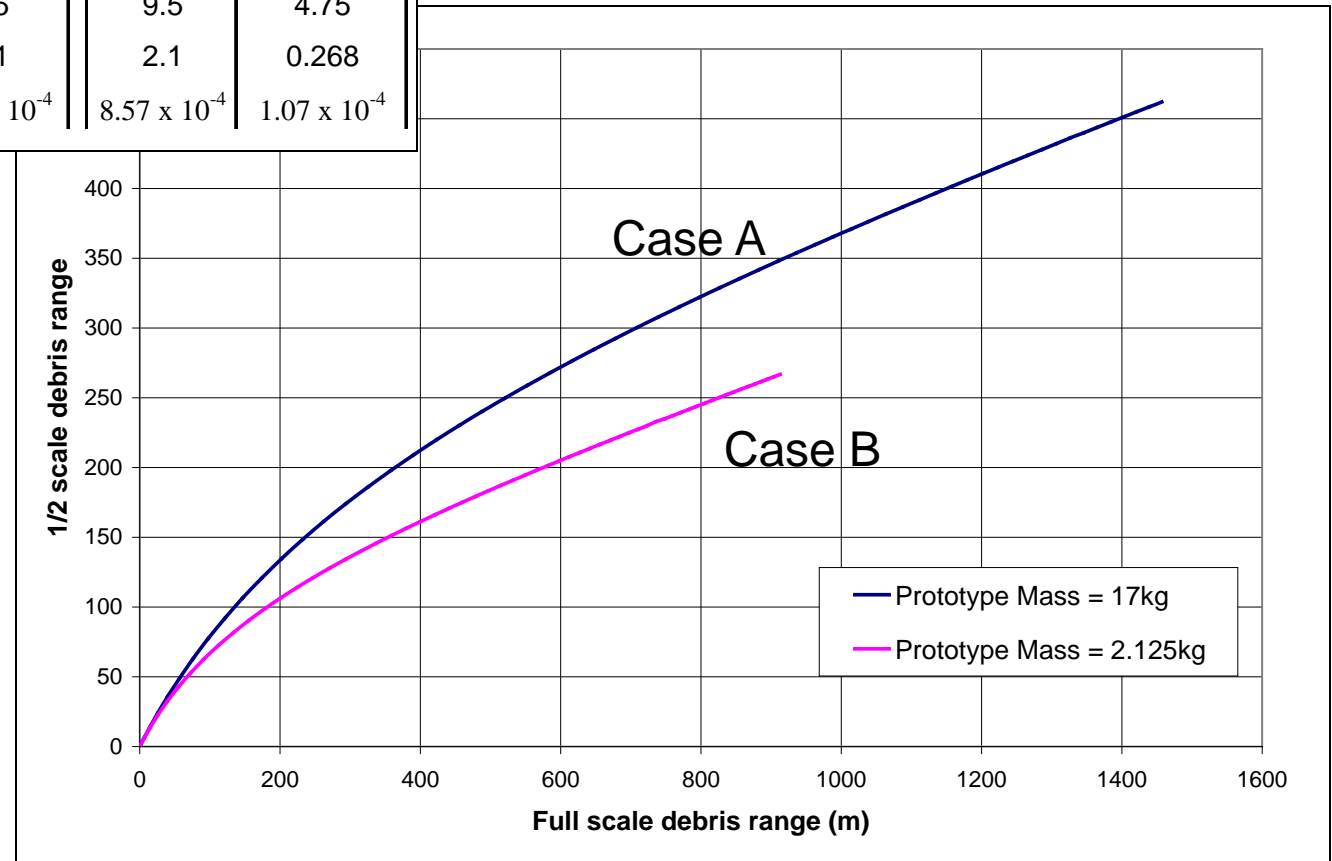- The debris range is more sensitive to the smaller debris mass (and size) compare to the larger debris mass.

Debris range vs. debris' mass

Size Effect on C_d

	Case A		Case B	
	Prototype	Half scale	Prototype	Half scale
Characteristic length (cm)	19	9.5	9.5	4.75
Mass (kg)	17.2	2.1	2.1	0.268
Volume (m^3)	0.007	8.57×10^{-4}	8.57×10^{-4}	1.07×10^{-4}

• Initial launch conditions : $v_0 = 60$m/s, $\theta_0 = 20^0$, $C_d = 1.2$

Distance relation between scaled debris

Debris bounce

Debris bounce criterion (based on Knock et al):

$V_f = 0$; $\vartheta_f = 0$ for $\vartheta_i \geq 13°$ and $V_i \geq 18$ m/s

$V_f = (1.0 - 0.00476\vartheta_i) V_i$ and $\vartheta_f = 0.484\vartheta_i$ **otherwise**

Incoming debris
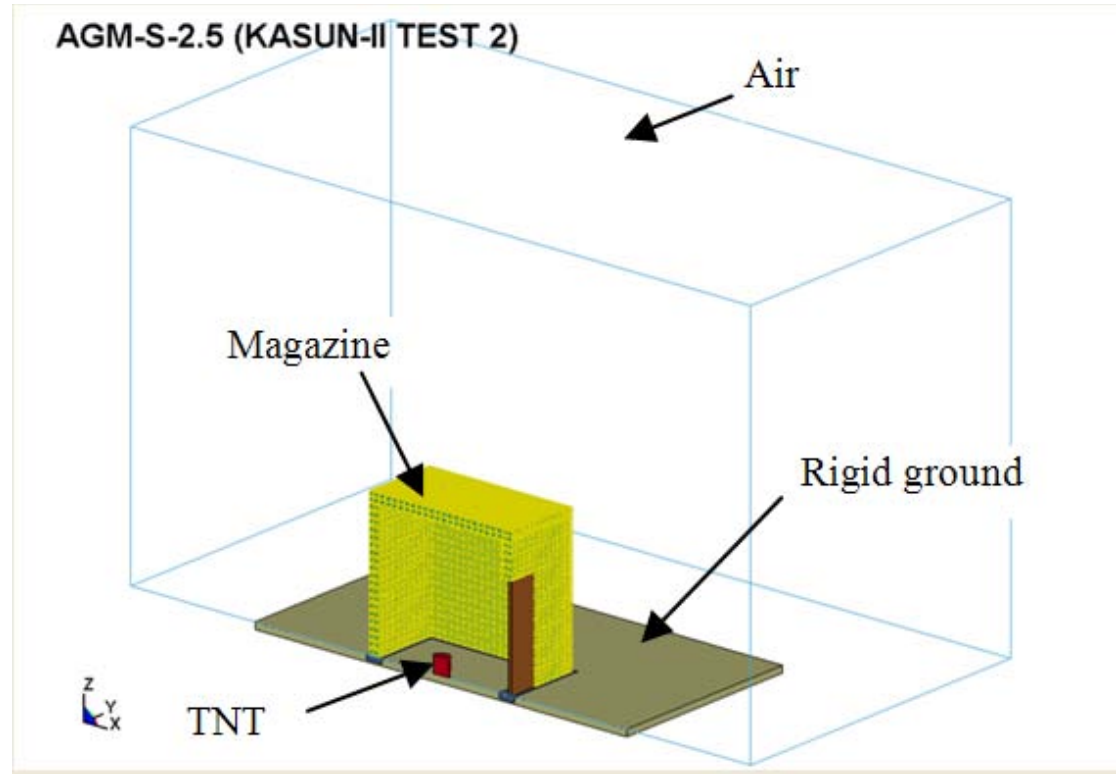Velocity = V_i

V_f

θ_i θ_f

Ground
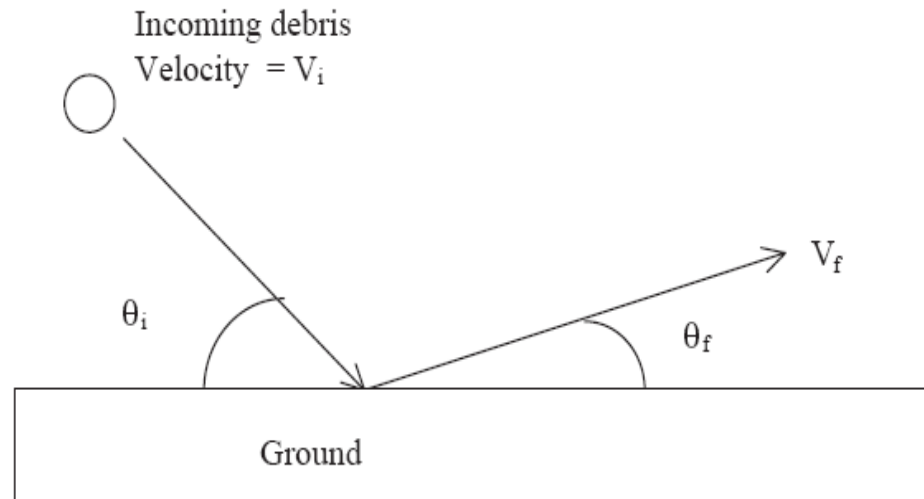
Case Study

- Based on one of the Kasun II test No 2.
- Comparison of modeling results with test
    - Comparison of velocity distribution
    - Comparison of vertical launch angle distribution
    - Comparison of debris dispersion map
    - Comparison of IBD (m)

Field test object and calculation model

Kasun II Test No 2

- Test conducted jointly by FOI and NDEA in 2006.

- 2m x 2m x 2m RC

- Wall & roof thickness = 0.15m

- ϕ12 rebar c/c both ways

- Bare charge = 20kg

- Loading density = 2.5kg/m^3

AGM-S-2.5 (KASUN-II TEST 2)

Air

Magazine

Rigid ground

TNT

Numerical model

Comparison of velocity distribution

Modeling
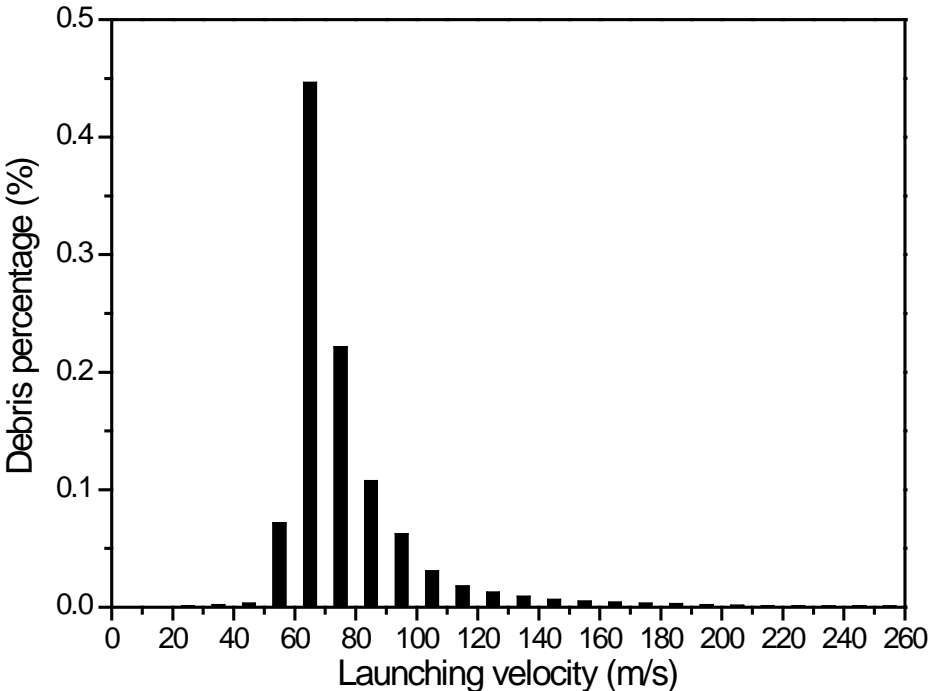
Test 2

Launching velocity by modeling
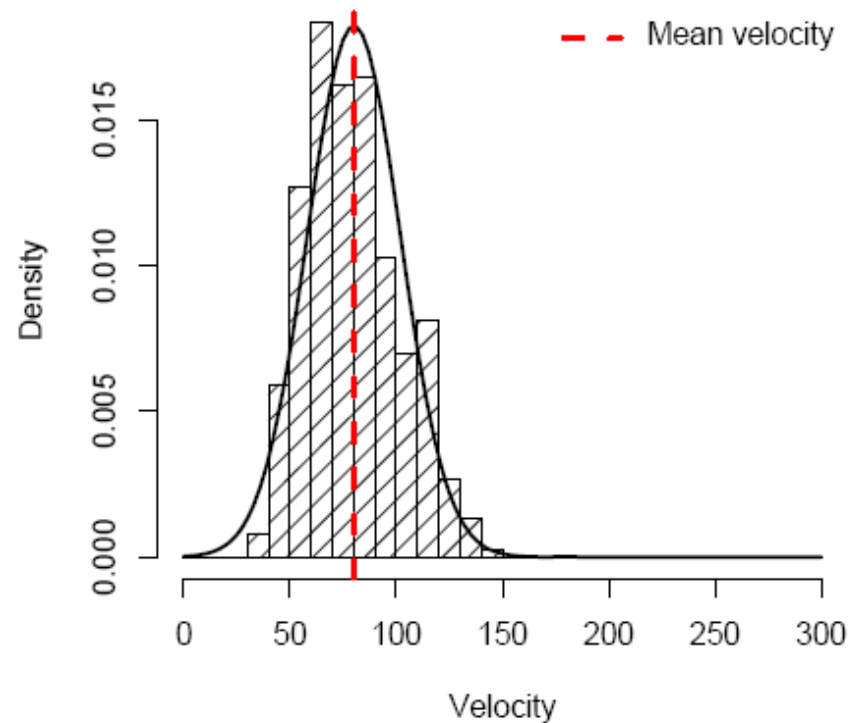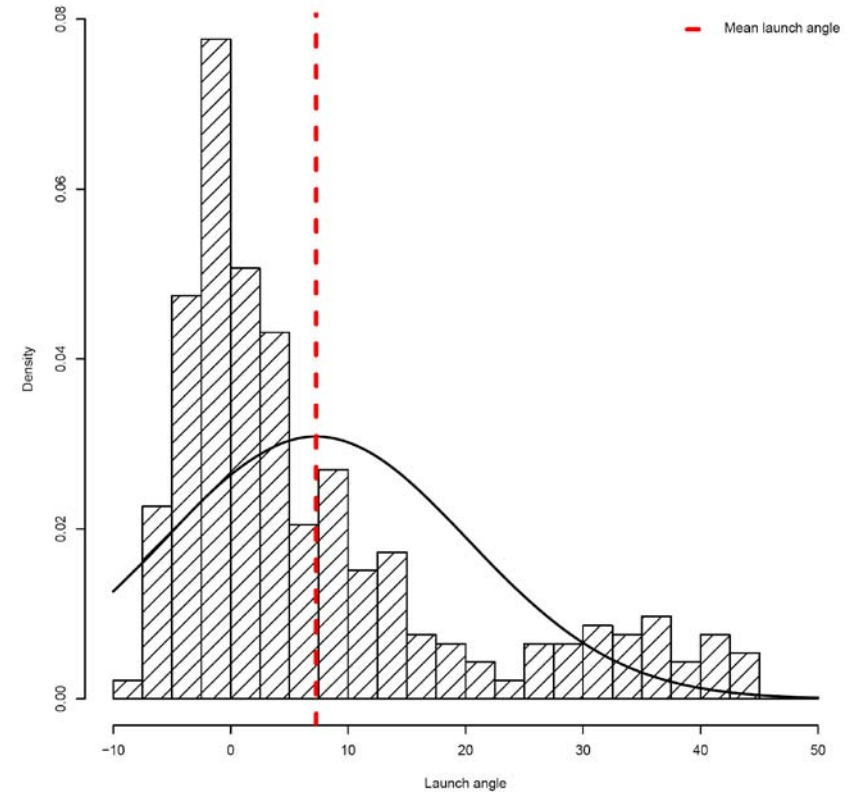
Launching velocity
by analysis of video record

Comparison of vertical launch angle distribution
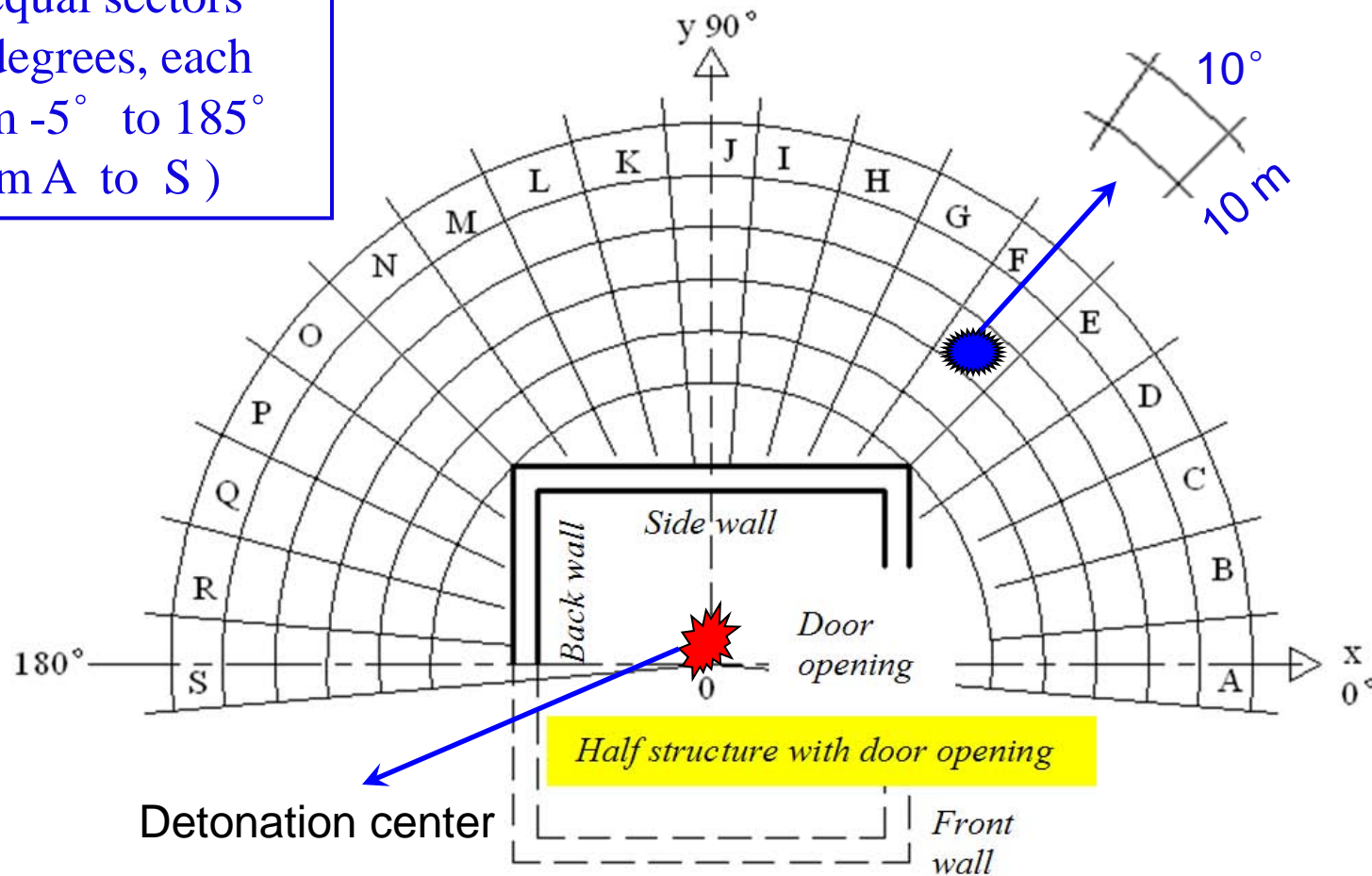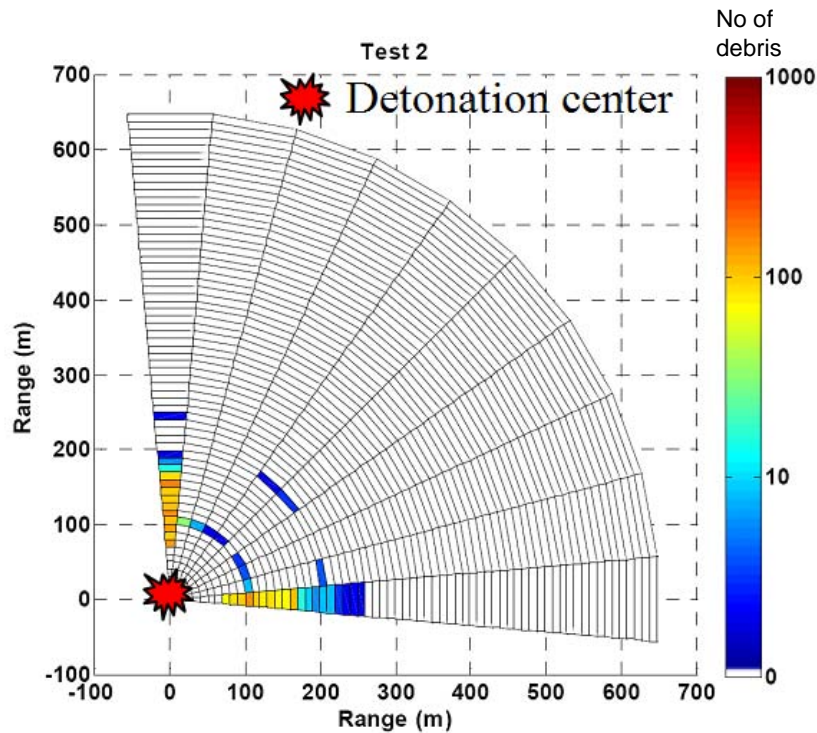

Modeling
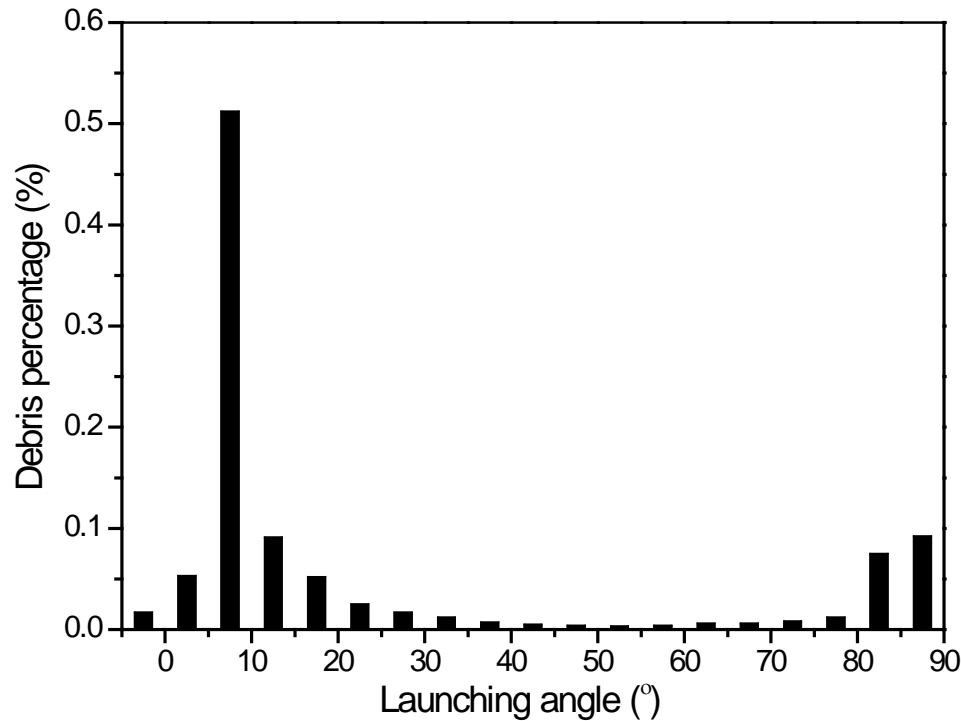
Launching angle by modeling

Launching angle
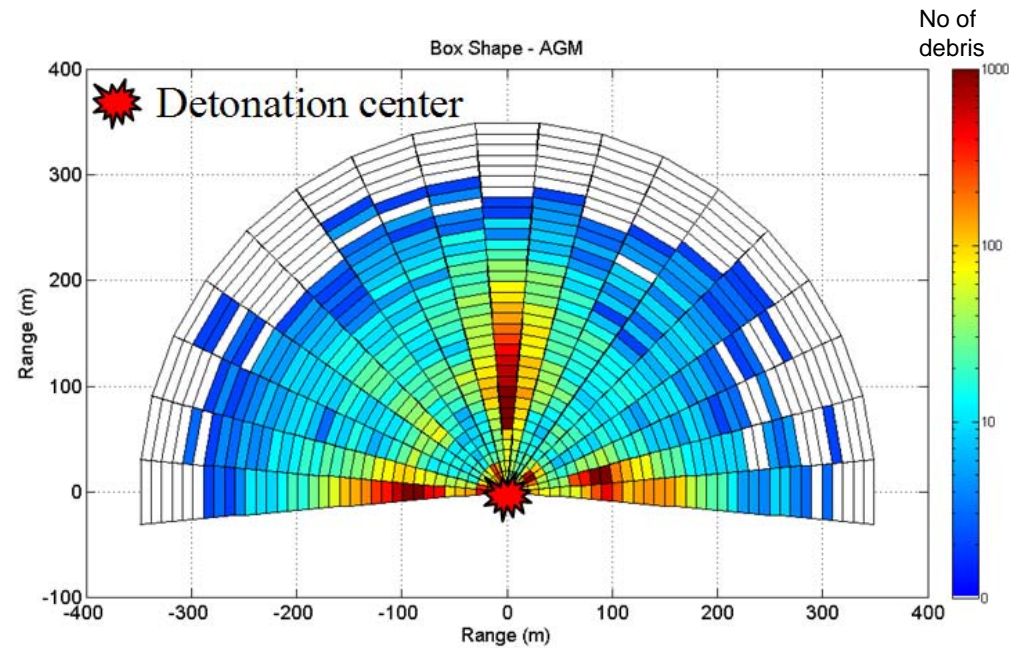by analysis of video record

Diagram of debris collecting sectors

- ➢ 19 equal sectors
- ➢ 10 degrees, each
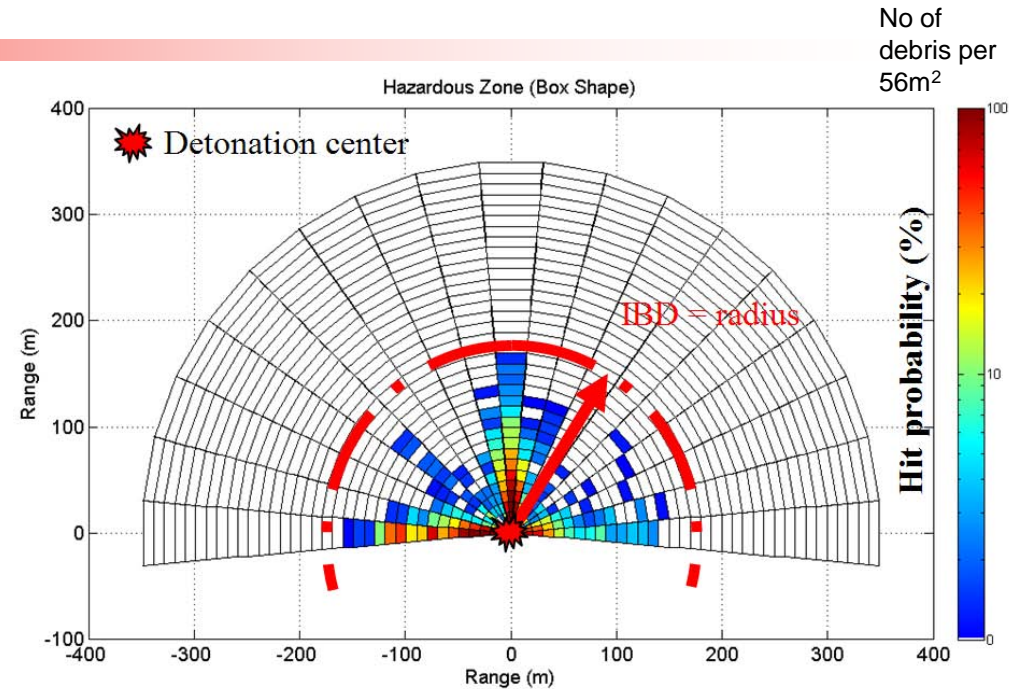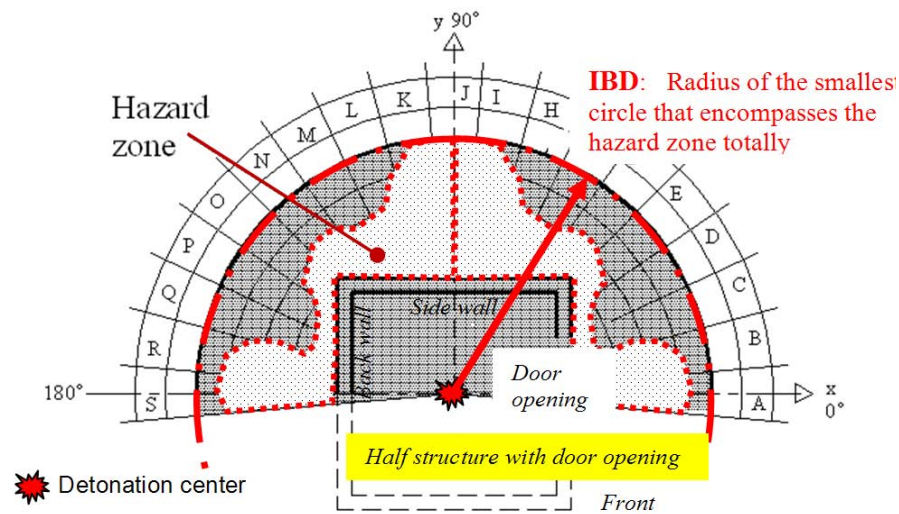- ➢ from -5° to 185°
  (from A to S)

Detonation center

Comparison of debris dispersion map

Kasun Test

Modeling with bounce twice

Collected debris from mass bin 1 – 8.

Debris IBD

Hazard zone

IBD: Radius of the smallest circle that encompasses the hazard zone totally

Side wall

Door opening

Half structure with door opening

Front

Detonation center

No of debris per 56m²

Hazardous Zone (Box Shape)

Detonation center

IBD = radius

Hit probability (%)

Comparison of IBD (m)

	Sector A (Front wall)	Sector J (Side wall)	Sector S (Back wall)	Global (Max)
Modelling	140	170	160	170
Kasun test	-	180	220	220

Future works

- More test could be simulated especially of higher loading density.

- Investigation works the debris trajectory and drag coefficient.

➔ Debris cluster effect

➔ Debris spinning effect

- Study of post impact problem : bounce, roll and further breakup upon impact.

- Effects of soil cover on internal loading and debris throw distance.

Questions ?